

Published in final edited form as:

Cell. 2013 January 17; 152(1-2): 262–275. doi:10.1016/j.cell.2012.11.052.

Derepression of a novel neuronal inhibitor is a major outcome of miRNA dysregulation due to 22q11.2 microdeletion

Bin Xu^{1,2,*}, Pei-Ken Hsu^{2,3,*}, Kimberly L. Stark^{1,2}, Maria Karayiorgou¹, and Joseph A. Gogos^{2,4}

¹Department of Psychiatry, College of Physicians and Surgeons, Columbia University, 1051 Riverside Drive, New York, New York 10032, USA

²Department of Physiology and Cellular Biophysics, College of Physicians and Surgeons, Columbia University, 630 West 168th Street, New York, New York 10032, USA

³Integrated Program in Cellular, Molecular, and Biophysical Studies, Columbia University, 630 West 168th Street, New York, New York 10032, USA

⁴Department of Neuroscience, College of Physicians and Surgeons, Columbia University, 1051 Riverside Drive, New York, New York 10032, USA

Summary

22q11.2 microdeletions result in specific cognitive deficits and schizophrenia. Analysis of *Df(16)A*^{+/-} mice, which model this microdeletion, revealed abnormalities in the formation of neuronal dendrites and spines, as well as altered brain microRNAs. Here we show a drastic reduction of *miR-185*, which resides within the 22q11.2 locus, to levels more than expected by a hemizygous deletion and demonstrate that this reduction alters dendritic and spine development. *miR-185* represses, through an evolutionary conserved target site, a previously unknown inhibitor of these processes that resides in the Golgi apparatus and shows higher prenatal brain expression. Sustained derepression of this inhibitor after birth represents the most robust transcriptional disturbance in the brains of *Df(16)A*^{+/-} mice and results in structural alterations in the hippocampus. Reduction of *miR-185* also has milder age and region-specific effects on the expression of a group of Golgi-related genes. Our findings illuminate the contribution of microRNAs in psychiatric disorders and cognitive dysfunction.

Introduction

The identification of a widespread role of chromosomal microdeletions and microduplications (copy-number variants or CNVs) in determining susceptibility to psychiatric disorders such as schizophrenia (SCZ), as well as neurodevelopmental disorders such as autism and intellectual disability, represents a shift in our understanding of the

© 2012 Elsevier Inc. All rights reserved

Correspondence should be addressed to M.K. (mk2758@columbia.edu) or J.A.G., (jag90@columbia.edu).

*These authors contributed equally to this work.

Author Contributions BX, P-KH, MK, JAG designed the research; BX, P-KH performed the experiments and analyzed the data; KLS contributed to the generation of the mouse strains; MK and JAG supervised experiments and data analysis; BX, P-KH, MK, JAG wrote the paper.

Expression profiling data Expression profiling data is available at Gene Expression Omnibus (GSE10784 and GSE29767).

Publisher's Disclaimer: This is a PDF file of an unedited manuscript that has been accepted for publication. As a service to our customers we are providing this early version of the manuscript. The manuscript will undergo copyediting, typesetting, and review of the resulting proof before it is published in its final citable form. Please note that during the production process errors may be discovered which could affect the content, and all legal disclaimers that apply to the journal pertain.

genetic architecture of these disorders and highlights the pervasive contribution of rare and highly penetrant structural mutations (Karayiorgou et al., 1995; Morrow, 2010; Rodriguez-Murillo et al., 2012). Along these lines, a strong link has been established between microdeletions in chromosome 22q11.2, cognitive dysfunction and psychiatric disorders, especially SCZ (Karayiorgou et al., 1995; Karayiorgou et al., 2010; Xu et al., 2008). Understanding how the genes disrupted by this deletion contribute to the ensuing psychiatric and cognitive phenotypes will provide important mechanistic insights and guide analysis of other pathogenic mutations (Arguello and Gogos, 2006, 2010, 2012; ISC, 2008; Karayiorgou et al., 2010).

By using chromosomal engineering, we generated a mouse model carrying a hemizygous 1.3-Mb chromosomal deficiency on mouse chromosome 16 [*Df(16)A*], which is syntenic to the 1.5-Mb 22q11.2 microdeletion (Stark et al., 2008). Analysis of *Df(16)A*^{+/-} mice showed abnormalities in dendritic morphogenesis and formation of dendritic spines of hippocampal pyramidal neurons both in culture and *in vivo* (Mukai et al., 2008; Stark et al., 2008). Such changes may account, at least in part, for the regional decreases in grey matter volumes observed in some 22q11.2 deletion carriers (Bearden et al., 2009; Chow et al., 2002) and may ultimately lead to altered information processing.

Analysis of the *Df(16)A*^{+/-} strain also provided compelling evidence that the 22q11.2 microdeletion results in abnormal processing of brain microRNAs (miRNAs), a class of small noncoding RNAs that regulate the stability and translation of mRNAs (Fineberg et al., 2009; Kosik, 2006; Schrott, 2009; Xu et al., 2010) implicating miRNA dysregulation in the pathogenesis of psychiatric disorders and cognitive dysfunction. One gene disrupted by the 22q11.2 microdeletion is *DGCR8*, a component of the “microprocessor” complex that is essential for miRNA production (Tomari and Zamore, 2005). *Dgcr8* haploinsufficiency results in the downregulation of a specific subset of mature miRNAs and contributes to alterations found in *Df(16)A*^{+/-} mice (Fenelon et al., 2011; Stark et al., 2008). miRNA dysregulation likely accounts for a fraction of the transcript misexpression in the brains of *Df(16)A*^{+/-} mice (Stark et al., 2008) but direct targets have not been reported. Here we highlight an important component of this dysregulation and identify a previously uncharacterized gene with prenatal expression bias as a major miRNA target mediating the effects of the 22q11.2 microdeletion on neuronal maturation and connectivity.

Results

A drastic reduction of *miR-185* levels in *Df(16)A*^{+/-} mice

Studies in the *Df(16)A*^{+/-} mouse strain have shown that the 22q11.2 microdeletion results in abnormal processing of a specific subset of brain miRNAs due to the removal of one copy of the *Dgcr8* gene causing a decrease in its expression in the adult brain (Stark et al., 2008) as well as in early development (Figure S1A). It is noteworthy that, in addition to *Dgcr8*, the 22q11.2 microdeletion and the equivalent mouse deficiency remove one copy of a miRNA gene (*miR-185*) located within the minimal 1.5-Mb 22q11.2 critical region (Figure 1A). *In situ* hybridization assays indicated that *miR-185* is expressed in several brain regions such as hippocampus (HPC) and cortex (Figure 1B). Quantitative real-time PCR (qRT-PCR) analysis showed that expression of *miR-185* is dramatically reduced by ~70–80% in both HPC ($P < 10^{-6}$) and prefrontal cortex (PFC, $P < 10^{-11}$) of adult *Df(16)A*^{+/-} mice as compared to wild type (Wt) littermates (Figures 1C–D). This reduction was also observed at earlier developmental stages [embryonic day 17 (E17) and postnatal day 6 (P6)] (Figure S1B). *miR-185* also showed a more modest decrease in *Dgcr8*^{+/-} mice (~20% in HPC, $P < 0.05$; Figure 1E) suggesting that the severe reduction of mature miR-185 expression in *Df(16)A*^{+/-} mice may be due to a combined effect of hemizygosity of the *miR-185* gene and impaired maturation of the pri-mir-185 transcript produced from the remaining copy, due to

the reduction in *Dgcr8* levels. Such a large reduction in expression of a resident gene to levels greater than expected by the 50% decrease in gene dosage is unique among genes affected by the 22q11.2 microdeletion.

A primary transcriptional consequence of 22q11.2 genomic loss

Previous microarray analysis of adult *Df(16)A^{+/-}* mice revealed genome-wide alterations of transcriptional programs in the HPC and PFC (Stark et al., 2008). We extended expression profile analysis of these two brain regions to two earlier developmental stages, E17 and P6. Only one gene, *2310044H10Rik*, was consistently significantly upregulated (in at least two of the three developmental stages examined and in at least one of the two brain areas tested). Indeed, *2310044H10Rik* was among the top upregulated genes in both postnatal stages examined (Figures 2A–B). Notably, no significant difference in *2310044H10Rik* expression was found in either frontal cortex or HPC at E17 (Figures 2A–B). Importantly, there is no known miRNA within or surrounding this genomic locus suggesting that the upregulation is not due to impaired processing of overlapping pri-miRNA transcripts.

In independent experiments, we attempted to distinguish primary versus secondary gene targets of the 22q11.2 microdeletion by looking for genes whose expression changes in opposite direction as a result of genomic losses or gains in this locus. Such genes are likely to represent primary targets and direct transcriptional readouts of the underlying copy number imbalances (Chahrour et al., 2008). We compared the PFC and HPC gene expression profiles in mice carrying a deletion or duplication at the 22q11.2 syntenic mouse locus using as reference compound heterozygous mice balanced for copy number (see Supplemental Methods and Figure S2). We identified a number of inversely altered transcripts in either PFC or HPC ($P < 0.001$, Supplemental Methods and Table S1), in addition to the transcripts from the 22q11.2 region. As expected, the majority of the identified transcripts are pri-miRNA forms. Only twelve transcripts were significantly misregulated in a reciprocal manner in both PFC and HPC (Table S2). Among them, *2310044H10Rik* is the only gene with protein coding potential.

Taken together, our expression profiling highlighted the misregulation of *2310044H10Rik* as a major consequence of the 22q11.2 genomic imbalances at the transcriptome level. We confirmed the pattern of *2310044H10Rik* upregulation in both PFC and HPC by TaqMan qRT-PCR (PFC: E17, 20%, $P = 0.24$; P6, 59%, $P < 0.01$; Adult, 76%, $P < 10^{-6}$; HPC: E17, 20%, $P = 0.16$; P6, 50%, $P < 0.05$; Adult, 38%, $P < 0.05$; Figures 2C–D). This analysis revealed a profile of temporal regulation with prenatal expression bias where levels of *2310044H10Rik* rapidly decline during the first week after birth and remain constantly low thereafter, as well as a corresponding pattern of misregulation in *Df(16)A^{+/-}* mice where prenatally elevated expression persists throughout postnatal and adult life. Increased brain expression of *2310044H10Rik* is recapitulated in *Df(16)A^{+/-}* primary neurons (Figure 2E).

2310044H10Rik is major downstream effector of miRNA dysregulation

Notably, *2310044H10Rik* mRNA levels were also elevated in *Dgcr8^{+/-}* mice (HPC: 30%, $P < 0.05$; PFC: 24%, $P < 0.05$; Figure S3A), suggesting that upregulation may be due to miRNA dysregulation. Indeed, two miRNA target site prediction programs, TargetScan (Grimson et al., 2007) and mirDB (Wang, 2008), report that the 3' UTR of *2310044H10Rik* contains binding sites of miRNAs shown to be affected in *Df(16)A^{+/-}* mice by microarray profiling (Stark et al., 2008). Specifically, mirDB predicted 5 such miRNAs with binding sites in the 3' UTR of *2310044H10Rik* including miR-185 and miR-485, whereas TargetScan predicted 13 miRNA sites, including sites for miR-185, miR-485, miR-491 and miR-224. Notably, both programs predicted sites for miR-185 and miR-485 (Figure 3A, red rectangles).

Because increased brain expression of *2310044H10Rik* is recapitulated in *Df(16)A^{+/-}* primary neurons (Figure 2E), we first used primary neurons to determine if endogenous *2310044H10Rik* expression is actually under the control of miR-185. To examine the effect of miR-185 overexpression on *2310044H10Rik* level, we introduced into primary neuronal cultures a miRNA precursor mimic (“pre-mir-185”), which is processed into mature miRNA, or a scramble precursor (“pre-scramble”) with no homology to the mouse genome, which serves as a control for nonspecific effects of small RNA expression. 24 hours post-transfection, there was a decrease in the levels of *2310044H10Rik* in pre-mir-185 transfected neurons when compared to pre-scramble transfected neurons ($P < 0.01$; Figure 3B). In a complementary experiment, introduction of an anti-miR-185 LNA oligo or a scramble control oligo resulted in an increase of *2310044H10Rik* mRNA levels in anti-miR-185 transfected cells when compared to scramble transfected cells ($P < 0.05$; Figure 3C). Taken together, these results confirm that *2310044H10Rik* expression in primary neurons is under the repressive control of miR-185. Essentially identical results were obtained when *2310044H10Rik* expression was assayed in N18 cells (Figures 3D–E). Therefore we used this cell line to further characterize the miR-185-mediated inhibition.

To test whether the inhibition of miR-185 on *2310044H10Rik* expression is 3' UTR-dependent as predicted by TargetScan and mirDB (see above), *2310044H10Rik* 3' UTR-fused luciferase reporter genes were co-transfected with either pre-mir-185 mimic or pre-scramble into N18 cells. While pre-scramble did not affect the reporter activity, introduction of pre-mir-185 mimic led to a dramatic decrease of luciferase activity as compared to the pre-scramble control ($P < 0.001$ for all pre-mir-185 concentrations used; Figure 3F). To investigate whether miR-185-mediated repression is specific and operates directly via the two binding sites predicted by TargetScan (Figure 3A), we engineered luciferase reporters carrying mutated versions of *2310044H10Rik* 3' UTR with either individual or both miR-185 binding sites mutated (Mut1:Site 1 mutant; Mut2:Site 2 mutant; Mut1&2:Site 1 and 2 mutants, see Supplemental Methods). The pre-mir-185 mimic significantly reduced the luciferase activity of the Wt reporter to ~25% relative to a control reporter without 3' UTR, while it reduced the luciferase activities of the Mut1 and Mut2 reporters to 80% ($P < 0.01$) and 33% ($P < 0.05$), respectively (Figure 3G). Notably, the pre-mir-185 mimic could not repress luciferase activity driven from a mutant reporter where both binding sites are simultaneously disrupted (Figure 3G). Thus, both miR-185 cognate binding sites have an impact on the 3' UTR-mediated regulation of *2310044H10Rik* expression, although the site disrupted in the Mut1 reporter (Site 1) seems to be the major target site via which miR-185 directly exerts its repressive effect.

We further addressed the dependence of *2310044H10Rik* 3' UTR reporter repression on the levels of miR-485 or miR-491, which are also predicted to target binding sites in the 3' UTR of the *2310044H10Rik* gene. Both of these miRNAs are modestly down-regulated in the HPC of the *Df(16)A^{+/-}* mice due to *Dgcr8* hemizyosity (Figure S3B). The pre-miRNA mimics of either miRNA modestly but significantly reduced the luciferase activity of the 3' UTR-fused reporter compared to the pre-scramble control (pre-mir-485: 27%, $P < 0.05$; pre-mir-491: 35%, $P < 0.05$; Figure 3H). A three-factor ANOVA analysis indicated that all three miRNAs (miR-185, miR-485 and miR-491) and their interactions have significant impact on the luciferase activity with the exception of the interaction between miR-485 and miR-491 (Table S3).

Taken together, these findings suggest that the persistent elevation of *2310044H10Rik* levels observed in *Df(16)A^{+/-}* mice is likely the result of the combined hemizyosity at *miR-185* and *Dgcr8* loci. Although more than one miRNA contributes, the major effect is due to the dramatic downregulation of miR-185. Consistent with this notion and the less profound reduction of miR-185 in *Dgcr8^{+/-}* mice (Figure 1E), *2310044H10Rik* is only modestly

upregulated in this strain (Figure S3A). Interestingly, a comparison between the 3' UTR of human and mouse orthologues (Figure 3A) reveals that miR-185 cognate Site 1 as well as one miR-485 binding site are located within a highly conserved region, suggesting that these sites are critical in regulating the levels of the human orthologue (*C19orf63*). Consistent with this expectation, introduction of pre-mir-185 into human 293T cells resulted in a significant decrease of endogenous *C19orf63* levels (Figure S3C). In addition, similar to the pattern observed in the mouse brain, expression of *C19orf63* decreases in infant brain as depicted in Brainspan database (www.brainspan.org).

It is noteworthy that inspection of our gene expression dataset as well as qRT-PCR analysis of a sample of eight high-likelihood miR-185 targets identified by more than one prediction program, did not reveal any additional significant changes of transcript levels in the brains of *Df(16)A^{+/-}* mice (Figure S3D). Furthermore, unlike *2310044H10Rik* none of the other top upregulated protein coding genes (shown in Figure 2B) are consistently altered in both HPC and frontal cortex of E17, P6 and adult *Df(16)A^{+/-}* mice and only one of them (*B3gat1*, see below) is predicted to contain miR-185 seed sites in its 3' UTR. Overall, although additional downstream targets of miR-185 likely exist (see below), our analysis suggests that *2310044H10Rik* represents the major downstream effector of miR-185 and a major hub target of miRNA dysregulation due to the 22q11.2 microdeletion. Due to confirmed miRNA-mediated regulation, we renamed the gene *Mirta22* (miRNA target of the 22q11.2 microdeletion).

***Mirta22* encodes a novel neuronal protein residing in the Golgi apparatus**

Mirta22 encodes a 28 kD protein without any known sequence homology or functional domain (<http://www.uniprot.org/uniprot/Q3TAS6>). The murine orthologue is located on mouse chromosome 7 and contains seven coding exons. The human orthologue (*C19orf63*) is located on chromosome 19q13.33 and encodes a protein with 92.3% identity to the murine protein (Figure 4A). One mouse reference sequence (isoform 1) is reported in GeneBank, while two *C19orf63* isoforms (isoform 1 and 2) are reported in GeneBank and in the literature (Junes-Gill et al., 2011). The protein encoded by isoform 1 is predicted to contain a N-terminal signal peptide, as well as a transmembrane segment (Figure 4A, red rectangles), which separates a long N-terminal region from a short C-terminal segment that contains a polyglycine tail with unknown function. Isoform 2 differs from isoform 1 by an alternatively spliced exon located after exon 6. The protein encoded by isoform 2 is shorter by 8 amino acids, contains the N-terminal signal peptide but not the transmembrane segment, and is predicted to be secreted (Figure 4A). We raised a polyclonal antibody against a segment of the protein that is conserved in the mouse and human orthologues (amino acids 207–226, Figure 4A, green rectangle; see Supplemental Methods and Figure S4). We validated the specificity of the antibody using a number of assays (see Supplemental Methods and Figures S4A–C) and showed that it can also detect the secreted form of the protein in 293T cell cultures (Figure S4D). Western blot assays of protein extracts from the brain of *Df(16)A^{+/-}* mice and Wt littermates showed the expected increase (25%) in *Mirta22* levels in mutant mice (Figure 4B). A similar in magnitude increase of the *Mirta22* immunocytochemical signal was observed in *Df(16)A^{+/-}* cultured neurons, as compared to Wt neurons (Figure 4C).

Immunostaining of neuronal cultures showed that *Mirta22* is primarily a neuronal protein (Figure 4D, upper panel). At the subcellular level, it is found primarily in the soma, where it colocalizes with the Golgi apparatus marker GM130 (Nakamura et al., 1995). As the neurons mature it is also found in vesicles and tubular-like clusters within the dendritic shafts (Figure 4D, middle panel). *Mirta22* immunoreactivity was not detected in cultures stained with preimmune serum (Figure S4E) and was diminished by 64% in *Mirta22* shRNA-transfected neurons (Figure S4F and S4G, lower panel). Immunohistochemical

analysis demonstrated that Mirta22 is widely distributed in the brain, where it is localized in neurons (Figure 4D, lower panel).

miR-185 reduction results in coordinated mild dysregulation of Golgi-related genes

Accumulating evidence suggests that miRNAs may target functionally connected genes, often in a developmental stage-specific manner (Tsang et al., 2010; Zhang et al., 2009). Consistent with this notion, functional annotation clustering analysis of 2695 out of 2708 predicted miR-185 targets (TargetScan Mouse v5.2) included in the DAVID *Mus musculus* gene functional annotation database (<http://david.abcc.ncifcrf.gov>) identified as the top enriched gene cluster (gene count = 159, Enrichment Score = 8.56, FDR-corrected $P = 2 \times 10^{-9}$) the Gene Ontology (cellular component) term “Golgi apparatus” (Figure 5A). Gene set enrichment analysis (GSEA) on the 2708 predicted miR-185 targets ranked based on the gene expression profile of *Df(16)A^{+/-}* mice also indicated that the Gene Ontology terms “Golgi apparatus part” and “Golgi apparatus” were among the top 20 gene sets in the adult HPC (Figure 5A). A global perspective on the enrichment of this miR-185 target gene set among the differentially expressed genes in the *Df(16)A^{+/-}* mice showed a significant enrichment in the adult HPC expression profile ($P = 5 \times 10^{-4}$) where, as expected, most of the top genes were upregulated ($n = 34$) and only 4 genes were downregulated at $P < 0.005$, Figure 5B and Table S4). A considerably more modest enrichment was suggested for the E17 ($P = 0.02$) and P6 HPC ($P = 0.016$) profiles (Figure S5). Interestingly, there was no significant enrichment within the PFC profiles in any of the three ages tested (E17: $P = 0.6311$; P6: $P = 0.1326$; Adult: $P = 0.244$). Expression changes were modest, with only 4/159 Golgi-related probe sets included among the top 100 in the adult HPC.

Altered miR-185 levels contribute to structural alterations of *Df(16)A^{+/-}* neurons

Df(16)A^{+/-} mice show impaired formation of dendrites and spines in the HPC (Mukai et al., 2008) and the PFC (Figure S6A–C), which are faithfully recapitulated in primary neuronal cultures. Impairment in these processes in *Df(16)A^{+/-}* mice could only be partially accounted for by the 50% decrease in the levels of Dgcr8 (Fenelon et al., 2011; Stark et al., 2008). Localization of Mirta22 within the Golgi apparatus and dendritic shafts suggests that diminishment of the miR-185 repression on Mirta22 levels may also contribute to these deficits.

To test this hypothesis we first asked whether reduction of miR-185 levels results in deficits in dendritic and spine development similar to those observed in *Df(16)A^{+/-}* neurons (Mukai et al., 2008). We introduced an anti-miR-185 and a scramble control LNA oligo into Wt primary hippocampal neurons and measured dendritic and spine morphology two days post-transfection at DIV9 and DIV19, respectively. Analysis of dendritic architecture indicated that reduction of miR-185 levels leads to deficits in dendritic complexity (Figure 6A), including a significant reduction in the number of primary dendrites (21%, $P < 0.05$; Figure 6B) and a significant reduction in total branch points in transfected neurons (16%, $P < 0.05$; Figure 6C). This finding was confirmed by Sholl analysis, which compares branch point numbers at varying distances from the soma (Figure S6D). Moreover, reduction of miR-185 levels in DIV19 neurons results in decreased spine density (21%, $P < 0.05$; Figures 6D–E and S6E) and a significant reduction in their median width (15% decrease, $P < 0.001$, Kolmogorov-Smirnov test; Figure 6F). Consistently, introduction of pre-mir-185 mimic into Wt neurons increased the number of primary dendrites, the number of branch points, the density and head width of mushroom spines (Figures S6F and S6G).

We also examined whether elevation of miR-185 levels could, at least partially, reverse cytoarchitectural alterations observed in *Df(16)A^{+/-}* neurons (Mukai et al., 2008). We transfected primary hippocampal neurons from *Df(16)A^{+/-}* mice and their Wt littermates

with pre-mir-185 or pre-scramble. A co-transfected GFP reporter plasmid allowed us to analyze the dendritic architecture (Figures 6G–I) and spine morphology (Figures 6J–L) of pyramidal neurons two days post-transfection at DIV9 and DIV19, respectively. Consistent with previous results (Mukai et al., 2008), compared to Wt neurons, *Df(16)A^{+/-}* neurons transfected with pre-scramble showed reduced dendritic complexity as manifested by a decrease in the number of primary dendrites (25%, $P < 10^{-10}$; Figure 6H) and number of dendritic branch points (38%, $P < 10^{-4}$; Figure 6I). They also showed reduced spine density (38%, $P < 10^{-6}$; Figure 6K) as well as a small, but statistically significant decrease in median head-width (8% decrease, $P < 0.01$; Figure 6L) of mushroom spines. Increase in miR-185 activity largely reversed the deficits in dendritic complexity (Figures 6H–I, S6H) and the reduction in spine density (Figures 6K, S6I) and increased the head-width of mushroom spines in *Df(16)A^{+/-}* hippocampal neurons (Figure 6L).

Elevation of Mirta22 levels inhibits dendritic and spine development in *Df(16)A^{+/-}* neurons

We examined whether elevation of Mirta22 levels could partially phenocopy the structural alterations observed in *Df(16)A^{+/-}* neurons (Mukai et al., 2008). We introduced a *Mirta22* cDNA into Wt primary hippocampal neurons and measured dendritic and spine morphology two days post-transfection, at DIV9 and DIV19 respectively. Control experiments using qRT-PCR and Western blot confirmed that the *Mirta22*-encoding plasmid drives increased expression of *Mirta22* at both mRNA and protein levels (Figures S7A–B). Analysis of dendritic architecture indicated that elevation of Mirta22 levels results in a significant reduction in the number of primary dendrites (18%, $P < 0.001$; Figure S7C) and total branch points in transfected neurons (41%, $P < 10^{-5}$; Figure S7D). This finding was confirmed by Sholl analysis (Figure S7E). Moreover, elevation of Mirta22 levels in DIV19 neurons results in decreased spine density (22%, $P < 0.05$; Figure S7F) and a small but significant reduction in the mushroom spine median width (8% decrease, $P < 0.001$, Kolmogorov-Smirnov test; Figure S7G). These structural deficits recapitulate those observed in *Df(16)A^{+/-}* neurons, suggesting these deficits are, at least in part, due to the aberrantly high levels of Mirta22.

We also asked whether reduction of Mirta22 levels could, at least partially, reverse cytoarchitectural alterations observed in *Df(16)A^{+/-}* neurons (Mukai et al., 2008). We transfected primary hippocampal neurons isolated from *Df(16)A^{+/-}* embryos and their Wt littermates with constructs that co-express turbo RFP (tRFP) and either a shRNA engineered to knock down expression of endogenous mouse Mirta22 or a scramble control shRNA (scr shRNA). We confirmed that the *Mirta22* shRNA can effectively knockdown the expression of *Mirta22* at both mRNA and protein levels (Figures S7H–I). We analyzed dendritic architecture and spine morphology two days following transfection, at DIV9 and DIV19 respectively. Introduction of *Mirta22* shRNA restored to Wt levels the number of primary dendrites of *Df(16)A^{+/-}* neurons at DIV9 (*Mirta22* shRNA versus scr shRNA, 40% increase, $P < 10^{-5}$; Figure 7A). A trend for increase in the total number of branch points in *Df(16)A^{+/-}* neurons was also observed (25% increase, $P = 0.16$; Figure S7J). Sholl analysis confirmed that introduction of *Mirta22* shRNA in *Df(16)A^{+/-}* neurons increased branch point numbers mainly in the proximal dendritic segments from the soma (Figure S7K). Furthermore, while DIV19 *Df(16)A^{+/-}* neurons transfected with the control shRNA had fewer and thinner mushroom spines than Wt neurons, introduction of *Mirta22* shRNA into *Df(16)A^{+/-}* neurons reversed the deficit in density (*Mirta22* shRNA versus scr shRNA, 91% increase, $P < 10^{-6}$; Figure 7B) while it had no significant impact on spine width (Figure 7C). The observation that reduction of Mirta22 levels partially reverses the structural deficits observed in *Df(16)A^{+/-}* mice was confirmed by using an independent *Mirta22* shRNA (Figures S7L–N) and strongly suggests that Mirta22 acts as an inhibitor mediating the effects of the structural mutation of dendritic and spine growth.

Reduction of *Mirta22* levels reverses structural alterations in the HPC of *Df(16)A*^{+/-} mice

To determine if *Mirta22* plays a role *in vivo*, we asked whether reduction of *Mirta22* levels reverses previously reported deficits in dendritic and spine formation at hippocampal CA1 pyramidal neurons of *Df(16)A*^{+/-} mice (Mukai et al., 2008). To this end, we used *Mirta22* mutant mice (2310044H10Rik^{Gt(OST181617)Lex/Mmucd}) carrying a retroviral gene trap insertion into intron 1 (Figure 7D). We confirmed that the insertion results in drastic reduction of *Mirta22* transcript and protein levels in the HPC of mutant mice (Figures 7E–F). We then crossed this line with *Df(16)A*^{+/-} mice to generate mice compound heterozygous for the *Df(16)A* and *Mirta22* mutations (*Df(16)A*^{+/-};*Mirta22*^{+/-}). Double mutants were compared to single mutants, as well as Wt littermates, to evaluate the contribution of *Mirta22* upregulation to the dendritic and spine phenotypes induced by *Df(16)A*. We used diolistics to sparsely label individual HPC neurons with DiI and analyzed dendritic and spine morphology in the CA1 subfield of all four genotypes using confocal imaging.

Our analysis confirms previously reported alterations in complexity and spine formation at the basal dendritic tree of CA1 pyramidal neurons of *Df(16)A*^{+/-} mice. Moreover, we show that presence of the *Mirta22* mutation in compound heterozygous *Df(16)A*^{+/-};*Mirta22*^{+/-} mice reverses to Wt levels the number of primary dendrites and total number of branch points (Figures 7G–I). Sholl analysis confirmed that reduction of *Mirta22* levels in *Df(16)A*^{+/-} mice results in increased dendritic branch point numbers (Figure 7J). Importantly, *Mirta22*^{+/-} mice did not differ significantly from Wt littermates in any of the tested parameters. Similarly, presence of the *Mirta22* mutation in compound heterozygous *Df(16)A*^{+/-};*Mirta22*^{+/-} mice reversed to almost Wt levels the *Df(16)A*-induced deficit in density and size of spines at the basal dendrites of CA1 neurons (Figure 7K–M). *Mirta22*^{+/-} mutants did not differ significantly from Wt littermates in these two parameters.

Discussion

Accumulating evidence suggests that miRNAs play an important role in the pathogenesis and pathophysiology of psychiatric disorders and cognitive dysfunction (Moreau et al., 2011; Stark et al., 2008; Xu et al., 2010). Here we provide a comprehensive view of the pattern of miRNA dysregulation emerging due to 22q11.2 deletions, which is shaped by the combined effect of *miR-185* and *Dgcr8* hemizyosity (see graphic summary). In this context, our results show a considerably greater reduction than the expected 50% decrease in the expression of a 22q11.2 gene indicating that mechanisms other than simple haploinsufficiency could represent an important and previously unappreciated component of CNV pathogenicity. Along these lines, our results also raise the intriguing possibility that 22q11.2 microdeletions, by partially disabling the miRNA machinery, create a sensitized genetic background, which promotes the effects of deleterious mutations that affect the expression or activity of a subset of miRNAs (Ambros, 2010; Brenner et al., 2010).

By comparing gene expression profiles over three developmental stages and three levels of genomic dosage at the 22q11.2 locus we identified elevated levels of a previously uncharacterized gene, *Mirta22*, as the most robust change in gene expression resulting from the 22q11.2 microdeletion, as well as the major downstream transcriptional effect of the 22q11.2-associated miRNA dysregulation. Localization of *Mirta22* in the Golgi apparatus and in vesicle and tubular-like extensions in dendrites is consistent with a role in membrane and protein trafficking and secretion, which is necessary for establishment and maintenance of neuronal connections (Evans et al., 2011; Horton et al., 2005; McAllister, 2000; Rosso et al., 2005; Wayman et al., 2006). *Mirta22* is likely to act in concert with other genes within the 22q11.2 deletion (Karayiorgou et al., 2010), including the *Zdhc8* palmitoyl-transferase, which is also located in the Golgi apparatus and modulates dendritic and spine development

(Mukai et al., 2008). Moreover, although *Mirta22* represents a major downstream effector of miR-185 dysregulation, our finding of a coordinated miR-185 targeting of Golgi apparatus-related genes suggests that *Mirta22* upregulation may act, in an age- and brain region-specific manner, in concert with other modestly altered miR-185 targets to interfere with the Golgi-related processes required for neuronal maturation. Thus, our findings highlight a link between the Golgi apparatus and neuronal phenotypes associated with the 22q11.2 microdeletion.

Mirta22 bias towards prenatal expression suggests that this gene may play an important role in both restricting neural circuit formation prenatally, when embryonically generated neurons are still migrating and extending their axons, and in permitting neuronal maturation and synaptogenesis to unfold in the postnatal brain, after neurons have migrated to their final destinations. Consistent with the notion that miRNAs function predominantly as fine-tuning regulators of the expression levels of their targets (Baek et al., 2008; Selbach et al., 2008), miR-185 and to a lesser extent other miRNAs affected by the 22q11.2 deletion appear to restrict and optimize *Mirta22* expression, presumably to avoid excessive inhibition during the critical stage of postnatal synapse formation. Accordingly, sustained derepression of the gene due to genomic loss at the 22q11.2 locus may have an impact on the formation of neural circuits in early postnatal development, as well on their maintenance during adulthood. Such structural changes could result in local and long-distance disruptions of neuronal communication (Fenelon et al., 2011; Sigurdsson et al., 2010) contributing to the cognitive dysfunction, psychiatric phenotypes or both. In agreement with this prediction, expression of the human orthologue of *Mirta22* (*C19orf63*) declines in infant brains (Kang et al., 2011).

It has been shown that during the transition between human fetal and infant development a large number of genes reverse their direction of expression from an increase in the first two trimesters *in utero* to a decrease in the third trimester [which corresponds to postnatal development in rodents (Clancy et al., 2007)] as well as after birth. ~40% of them are predicted miRNA targets (Colantuoni et al., 2011; Xu et al., 2012). In that respect, *Mirta22* is one example of a disease-related gene representative of this type of transcriptional trajectory indicative of a miRNA-imposed temporal control over the sequential maturation of neurons, synapses and circuits. Analysis of common variation in the vicinity of the human orthologue (Ripke et al., 2011) identified one SNP (rs10401266) 35Kb upstream of *C19orf63* in a presumptive regulatory region with nominally significant association with SCZ ($P = 5 \times 10^{-3}$). The impact of rare variants in *C19orf63* remains to be determined, but importantly, we recently provided evidence that rare *de novo* deleterious mutations in genes showing a prenatal expression bias and miRNA regulation similar to *Mirta22* are enriched in individuals with SCZ, especially those with prominent early prepsychotic, deviant behaviors (Gilman et al., 2012; Xu et al., 2012). Overall, understanding how *Mirta22* affects neuronal connectivity and eventually behavior and cognition is likely to provide more general insights into the contribution of miRNAs in psychiatric and neurodevelopmental disorders, illuminate the patterns of neural complexity underlying these disorders and facilitate development of new treatments.

Experimental Procedures

Mutant mice

Df(16)A^{+/-} and *Dgcr8^{+/-}* mice have been described previously (Stark et al., 2008; Mukai et al., 2008) and have been backcrossed into C57BL/6J background for over 10 generations. *Mirta22* mutant mice (*2310044H10Rik^{Gt(OST181617)Lex⁺}Mmucd*, referred to as *Mirta22^{+/-}*) were obtained from the Mutant Mouse Regional Resource Centers supported by NIH (MMRRC).

qRT-PCR and expression profiling

Total RNA was isolated by miRNeasy mini kit. qRT-PCR was performed as described previously (Stark et al., 2008). For expression profiling, cDNA was generated and exposed to the Affymetrix Mouse genome 430 2.0 array, which includes 45,000 probe sets from > 34,000 well-characterized mouse genes. Data was obtained using GeneChip Analysis Software Microarray Suite version 5 and analyzed with limma package in the bioconductor project (www.bioconductor.org). Details provided in Supplemental Methods.

Analysis of dendritic complexity and spine morphology

Dissected E17 hippocampal neurons were plated at 2×10^5 cells/ml in 6-well plates, cultured for 9–19 days and transfected with GFP or RFP plasmids depending on the experiment. CA1 pyramidal neurons were sparsely labeled using diolistic labeling (see Supplemental Methods). Images of dendrites and dendritic spines were acquired as described previously (Mukai et al., 2008). An experimenter blind to the genotype performed imaging and analysis. Details provided in Supplemental Methods.

Luciferase assays

Mirta22 3' UTR was cloned into psiCHECK2. Binding site mutant clones were generated by PCR-based mutagenesis. N18 neuroblastoma cells were transfected with various psiCHECK2 reporter constructs together with pre-mir-185 mimic or pre-scramble control unless mentioned otherwise and luciferase assays were performed using the Promega Dual-Luciferase Reporter Assay System. All experiments were performed at least 2 times and all data presented is the average of 3 technical repeats. Details provided in Supplemental Methods.

Functional enrichment analysis of predicted *miR-185* targets

miR-185 target gene list was imported into DAVID gene functional annotation database. Functional annotation was conducted using the program's functional annotation clustering analysis with default settings. Geneset enrichment analysis (GSEA) was conducted using GSEA v2.0. Details provided in Supplemental Methods.

Antibodies

A 20 amino acid peptide ([C]-CEQAQKAKNPQEQKSFFAKY-[N]) was used to generate a rabbit polyclonal antibody. Western blot, immunohistochemistry and immunocytochemistry assays were conducted as previously described (Mukai et al., 2008; Stark et al., 2008). Details provided in Supplemental Methods.

Supplementary Material

Refer to Web version on PubMed Central for supplementary material.

Acknowledgments

We thank Yan Sun, Merilee Teylan, Xuanyi Zou and Megan Sribour for support with the maintenance of the mouse colony and technical assistance. We are also grateful to Drs. David Sulzer and Guomei Tang for their kind help with the diolistic assays. We thank Drs. Jun Mukai and Mirna Kvajo for help and insights with the immunocytochemistry assays. We also thank Dr. Mirna Kvajo and Rebecca Levy for critical reading of the manuscript. This work was supported by a grant from the Simons Foundation (to J.A.G.), US National Institute of Mental Health grants MH67068 (to M.K. and J.A.G.), MH077235 and MH97879 (to J.A.G.), and by grants from the March of Dimes Foundation and the McKnight Endowment Fund for Neuroscience (to M.K.); B.X. was supported in part by a National Alliance for Research on Schizophrenia and Depression (NARSAD) Young Investigator Award. K.L.S. was supported by a NARSAD Suzanne and John Golden Young Investigator Award.

References

- Ambros V. MicroRNAs: genetically sensitized worms reveal new secrets. *Curr Biol.* 2010; 20:R598–600. [PubMed: 20656201]
- Arguello PA, Gogos JA. Modeling madness in mice: one piece at a time. *Nuron.* 2006; 52:179–196.
- Arguello PA, Gogos JA. Cognition in mouse models of schizophrenia susceptibility genes. *Schizophr Bull.* 2010; 36:289–300. [PubMed: 20026558]
- Arguello PA, Gogos JA. Genetic and cognitive windows into circuit mechanisms of psychiatric disease. *Trends Neurosci.* 2012; 35:3–13. [PubMed: 22177981]
- Baek D, Villen J, Shin C, Camargo FD, Gygi SP, Bartel DP. The impact of microRNAs on protein output. *Nature.* 2008; 455:64–71. [PubMed: 18668037]
- Bearden CE, van Erp TG, Dutton RA, Lee AD, Simon TJ, Cannon TD, Emanuel BS, McDonald-McGinn D, Zackai EH, Thompson PM. Alterations in midline cortical thickness and gyrification patterns mapped in children with 22q11.2 deletions. *Cereb Cortex.* 2009; 19:115–126. [PubMed: 18483006]
- Brenner JL, Jasiewicz KL, Fahley AF, Kemp BJ, Abbott AL. Loss of individual microRNAs causes mutant phenotypes in sensitized genetic backgrounds in *C. elegans*. *Curr Biol.* 2010; 20:1321–1325. [PubMed: 20579881]
- Chahour M, Jung SY, Shaw C, Zhou X, Wong ST, Qin J, Zoghbi HY. MeCP2, a key contributor to neurological disease, activates and represses transcription. *Science.* 2008; 320:1224–1229. [PubMed: 18511691]
- Chow EW, Zipursky RB, Mikulis DJ, Bassett AS. Structural brain abnormalities in patients with schizophrenia and 22q11 deletion syndrome. *Biological Psychiatry.* 2002; 51:208–215. [PubMed: 11839363]
- Clancy B, Finlay BL, Darlington RB, Anand KJ. Extrapolating brain development from experimental species to humans. *Neurotoxicology.* 2007; 28:931–937. [PubMed: 17368774]
- Colantuoni C, Lipska BK, Ye T, Hyde TM, Tao R, Leek JT, Colantuoni EA, Elkahoulou AG, Herman MM, Weinberger DR, et al. Temporal dynamics and genetic control of transcription in the human prefrontal cortex. *Nature.* 2011; 478:519–523. [PubMed: 22031444]
- Evans SF, Irmady K, Ostrow K, Kim T, Nykjaer A, Saftig P, Blobel C, Hempstead BL. Neuronal brain-derived neurotrophic factor is synthesized in excess, with levels regulated by sortilin-mediated trafficking and lysosomal degradation. *J Biol Chem.* 2011; 286:29556–29567. [PubMed: 21730062]
- Fenelon K, Mukai J, Xu B, Hsu PK, Drew LJ, Karayiorgou M, Fischbach GD, Macdermott AB, Gogos JA. Deficiency of *Dgcr8*, a gene disrupted by the 22q11.2 microdeletion, results in altered short-term plasticity in the prefrontal cortex. *Proc Natl Acad Sci U S A.* 2011; 108:4447–4452. [PubMed: 21368174]
- Fineberg SK, Kosik KS, Davidson BL. MicroRNAs potentiate neural development. *Neuron.* 2009; 64:303–309. [PubMed: 19914179]
- Gilman S, Chang J, Xu B, Bawa T, Gogos JA, Karayiorgou M, Vitkup D. Diverse types of genetic variation converge on functional gene networks involved in schizophrenia. *Nature neuroscience.* 2012 In Press.
- Grimson A, Farh KK, Johnston WK, Garrett-Engele P, Lim LP, Bartel DP. MicroRNA targeting specificity in mammals: determinants beyond seed pairing. *Mol Cell.* 2007; 27:91–105. [PubMed: 17612493]
- Horton AC, Racz B, Monson EE, Lin AL, Weinberg RJ, Ehlers MD. Polarized secretory trafficking directs cargo for asymmetric dendrite growth and morphogenesis. *Neuron.* 2005; 48:757–771. [PubMed: 16337914]
- ISC. Rare chromosomal deletions and duplications increase risk of schizophrenia. *Nature.* 2008; 455:237–241. [PubMed: 18668038]
- Junes-Gill KS, Gallaher TK, Gluzman-Poltorak Z, Miller JD, Wheeler CJ, Fan X, Basile LA. hHSS1: a novel secreted factor and suppressor of glioma growth located at chromosome 19q13.33. *J Neurooncol.* 2011; 102:197–211. [PubMed: 20680400]

- Kang HJ, Kawasawa YI, Cheng F, Zhu Y, Xu X, Li M, Sousa AM, Pletikos M, Meyer KA, Sedmak G, et al. Spatio-temporal transcriptome of the human brain. *Nature*. 2011; 478:483–489. [PubMed: 22031440]
- Karayiorgou M, Morris MA, Morrow B, Shprintzen RJ, Goldberg R, Borrow J, Gos A, Nestadt G, Wolyniec PS, Lasseter VK, et al. Schizophrenia susceptibility associated with interstitial deletions of chromosome 22q11. *Proc Natl Acad Sci U S A*. 1995; 92:7612–7616. [PubMed: 7644464]
- Karayiorgou M, Simon TJ, Gogos JA. 22q11.2 microdeletions: linking DNA structural variation to brain dysfunction and schizophrenia. *Nat Rev Neurosci*. 2010; 11:402–416. [PubMed: 20485365]
- Kosik KS. The neuronal microRNA system. *Nat Rev Neurosci*. 2006; 7:911–920. [PubMed: 17115073]
- McAllister AK. Cellular and molecular mechanisms of dendrite growth. *Cereb Cortex*. 2000; 10:963–973. [PubMed: 11007547]
- Moreau MP, Bruse SE, David-Rus R, Buyske S, Brzustowicz LM. Altered microRNA expression profiles in postmortem brain samples from individuals with schizophrenia and bipolar disorder. *Biol Psychiatry*. 2011; 69:188–193. [PubMed: 21183010]
- Morrow EM. Genomic copy number variation in disorders of cognitive development. *J Am Acad Child Adolesc Psychiatry*. 2010; 49:1091–1104. [PubMed: 20970697]
- Mukai J, Dhillia A, Drew LJ, Stark KL, Cao L, MacDermott AB, Karayiorgou M, Gogos JA. Palmitoylation-dependent neurodevelopmental deficits in a mouse model of 22q11 microdeletion. *Nat Neurosci*. 2008; 11:1302–1310. [PubMed: 18836441]
- Nakamura N, Rabouille C, Watson R, Nilsson T, Hui N, Slusarewicz P, Kreis TE, Warren G. Characterization of a cis-Golgi matrix protein, GM130. *J Cell Biol*. 1995; 131:1715–1726. [PubMed: 8557739]
- Ripke S, Sanders AR, Kendler KS, Levinson DF, Sklar P, Holmans PA, Lin DY, Duan J, Ophoff RA, Andreassen OA, et al. Genome-wide association study identifies five new schizophrenia loci. *Nat Genet*. 2011
- Rodriguez-Murillo L, Gogos JA, Karayiorgou M. The genetic architecture of schizophrenia: new mutations and emerging paradigms. *Annu Rev Med*. 2012; 63:63–80. [PubMed: 22034867]
- Rosso SB, Sussman D, Wynshaw-Boris A, Salinas PC. Wnt signaling through Dishevelled, Rac and JNK regulates dendritic development. *Nat Neurosci*. 2005; 8:34–42. [PubMed: 15608632]
- Schratt G. microRNAs at the synapse. *Nat Rev Neurosci*. 2009; 10:842–849. [PubMed: 19888283]
- Selbach M, Schwanhaussner B, Thierfelder N, Fang Z, Khanin R, Rajewsky N. Widespread changes in protein synthesis induced by microRNAs. *Nature*. 2008; 455:58–63. [PubMed: 18668040]
- Sigurdsson T, Stark KL, Karayiorgou M, Gogos JA, Gordon JA. Impaired hippocampal-prefrontal synchrony in a genetic mouse model of schizophrenia. *Nature*. 2010; 464:763–767. [PubMed: 20360742]
- Stark KL, Xu B, Bagchi A, Lai WS, Liu H, Hsu R, Wan X, Pavlidis P, Mills AA, Karayiorgou M, et al. Altered brain microRNA biogenesis contributes to phenotypic deficits in a 22q11-deletion mouse model. *Nat Genet*. 2008; 40:751–760. [PubMed: 18469815]
- Tomari Y, Zamore PD. MicroRNA biogenesis: drosha can't cut it without a partner. *Curr Biol*. 2005; 15:R61–64. [PubMed: 15668159]
- Tsang JS, Ebert MS, van Oudenaarden A. Genome-wide dissection of microRNA functions and cotargeting networks using gene set signatures. *Mol Cell*. 2010; 38:140–153. [PubMed: 20385095]
- Wang X. miRDB: a microRNA target prediction and functional annotation database with a wiki interface. *RNA*. 2008; 14:1012–1017. [PubMed: 18426918]
- Wayman GA, Impey S, Marks D, Saneyoshi T, Grant WF, Derkach V, Soderling TR. Activity-dependent dendritic arborization mediated by CaM-kinase I activation and enhanced CREB-dependent transcription of Wnt-2. *Neuron*. 2006; 50:897–909. [PubMed: 16772171]
- Xu B, Ionita-Laza I, Roos JL, Boone B, Woodrick S, Sun Y, Levy S, Gogos JA, Karayiorgou M. De novo gene mutations highlight patterns of genetic and neural complexity in schizophrenia. *LID*. 201210.1038/ng.2446 [doi]
- Xu B, Karayiorgou M, Gogos JA. MicroRNAs in psychiatric and neurodevelopmental disorders. *Brain Res*. 2010; 1338:78–88. [PubMed: 20388499]

- Xu B, Roos JL, Levy S, van Rensburg EJ, Gogos JA, Karayiorgou M. Strong association of de novo copy number mutations with sporadic schizophrenia. *Nat Genet.* 2008; 40:880–885. [PubMed: 18511947]
- Zhang L, Hammell M, Kudlow BA, Ambros V, Han M. Systematic analysis of dynamic miRNA-target interactions during *C. elegans* development. *Development.* 2009; 136:3043–3055. [PubMed: 19675127]

\$watermark-text

\$watermark-text

\$watermark-text

Highlights

- A mouse model of the hemizygous 22q11.2 deletion shows over 50% reduction of *miR-185*
- *Mirta22* is a miR-185 target and a major effector of the 22q11.2 miRNA dysregulation
- *Mirta22* is a prenatally-biased neuronal inhibitor located in the Golgi apparatus
- Altered levels of miR-185 and *Mirta22* affect dendrite and spine development

\$watermark-text

\$watermark-text

\$watermark-text

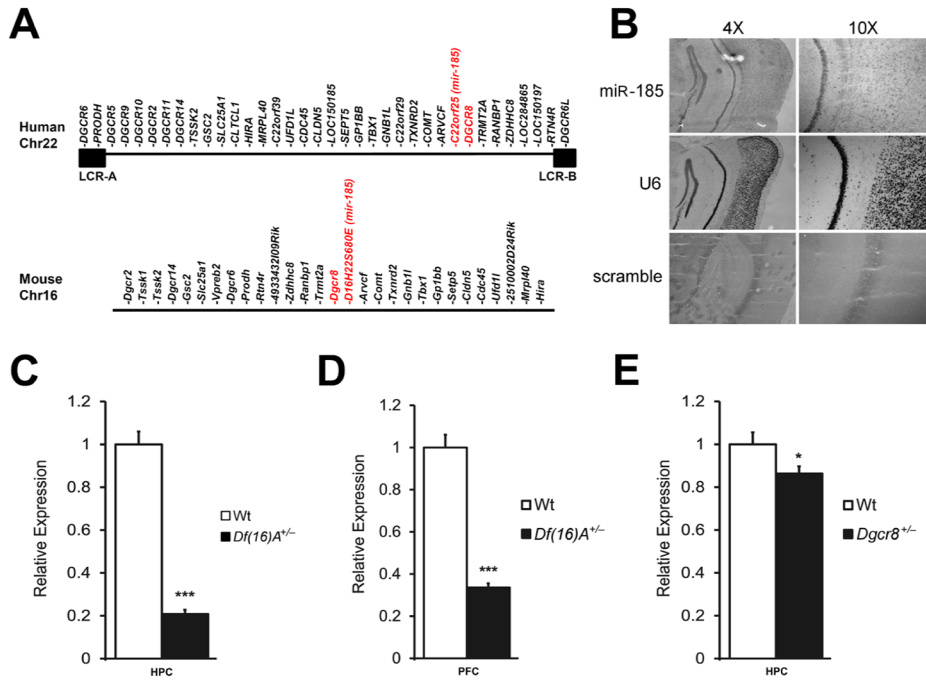


Figure 1. Drastic reduction of *mir-185* expression in *Df(16)A^{+/-}* mice

(A) Schematic diagram showing the 1.5-Mb 22q11.2 critical region and the syntenic mouse locus. The 1.5-Mb deletion is mediated by low copy repeat sequences LCR-A and LCR-B (illustrated as black boxes). *Dgcr8* and *miR-185* (hosted in the intron of the *22orf25* gene in human and the *D16H22S680E* gene in mouse) are highlighted in red.

(B) Expression of *miR-185* mRNA in HPC and cortex as shown by *in situ* hybridization in coronal brain sections using an antisense *miR-185* probe. An antisense U6 probe and a scramble probe were used as positive and negative controls, respectively. Images were taken at either 4X (left panels) or 10X (right panels) magnification.

(C–E) *miR-185* expression levels in HPC (C) or PFC (D) of *Df(16)A^{+/-}* ($n = 7$ for mutant, $n = 9$ for Wt) and in HPC (E) of *Dgcr8^{+/-}* ($n = 10$ for mutant and Wt), as assayed by qRT-PCR. Expression levels in mutant mice were normalized to their respective Wt littermates. Results are expressed as mean \pm SEM. * $P < 0.05$, ** $P < 0.01$, *** $P < 0.001$ (Student's *t*-test). See also Figure S1.

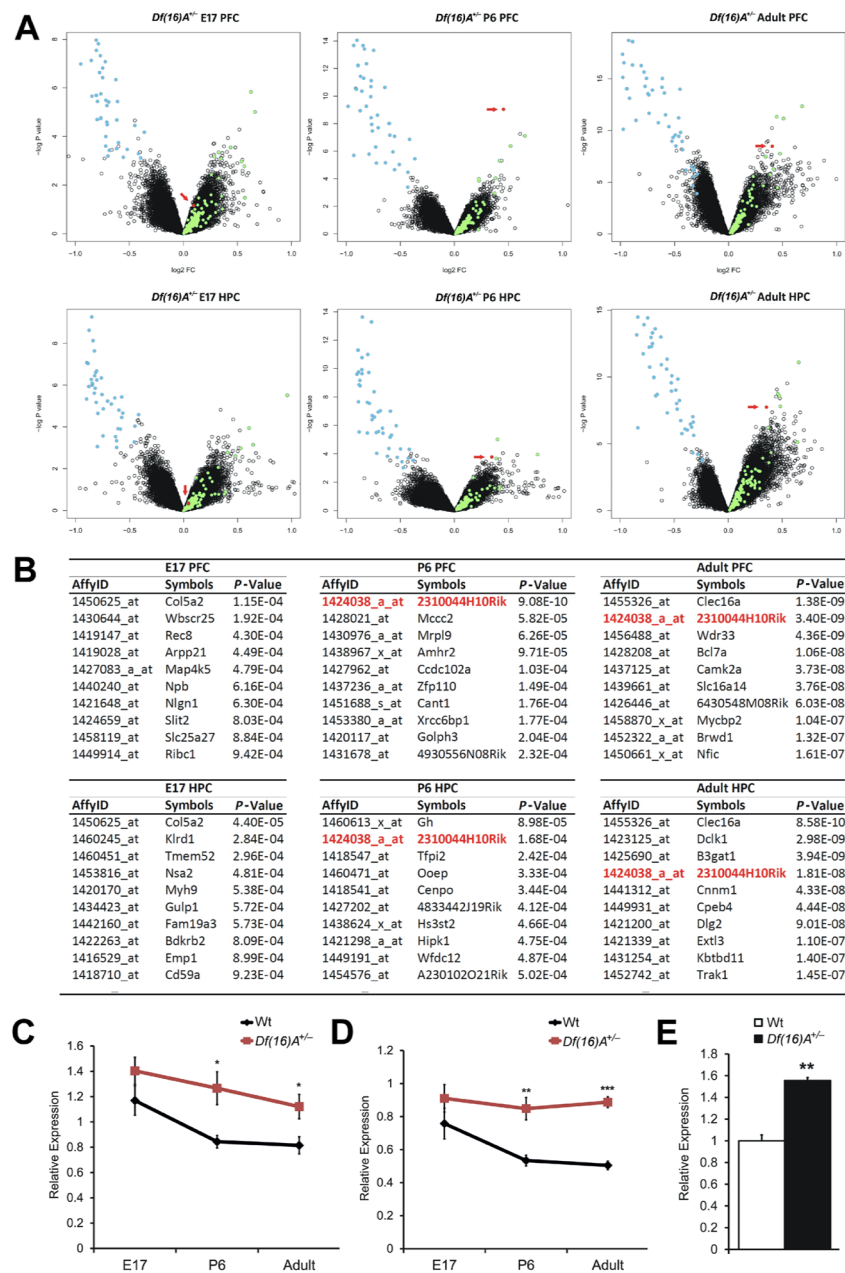


Figure 2. 2310044H10Rik (*Mirta22*) is robustly upregulated in the brain of *Df(16)A^{+/-}* mice
 (A) Changes in gene expression in the PFC (upper panel) or HPC (lower panel) of *Df(16)A^{+/-}* and Wt littermate control mice at E16, P6 and adulthood ($n = 10$ each group): Volcano plot of the P -values and the corresponding relative expression of each gene. Light blue dots indicate genes within *Df(16)A* deficiency; light green dots indicate upregulated miRNA-containing transcripts; red dots indicate probe sets representing *Mirta22*.
 (B) Top 10 protein encoding genes that show significant upregulation in the PFC (upper panel) or HPC (lower panel) of *Df(16)A^{+/-}* and Wt littermate mice at E16, P6 and adulthood. *Mirta22* is highlighted in red.
 (C, D) Temporal expression of *2310044H10Rik (Mirta22)* in the PFC (C) and HPC (D) of *Df(16)A^{+/-}* and Wt littermate mice as monitored by qRT-PCR. $n = 9-10$ for each group.

(E) Increased expression of endogenous *2310044H10Rik (Mirta22)* in DIV9 hippocampal neurons isolated from *Df(16)A^{+/-}* animals as assayed by qRT-PCR ($n = 3$ each genotype). Expression levels in mutant neurons were normalized to Wt neurons. Results are expressed as mean \pm SEM. * $P < 0.05$, ** $P < 0.01$, *** $P < 0.001$ (Student's t -test). See also Figure S2, Tables S1 and S2.

\$watermark-text

\$watermark-text

\$watermark-text

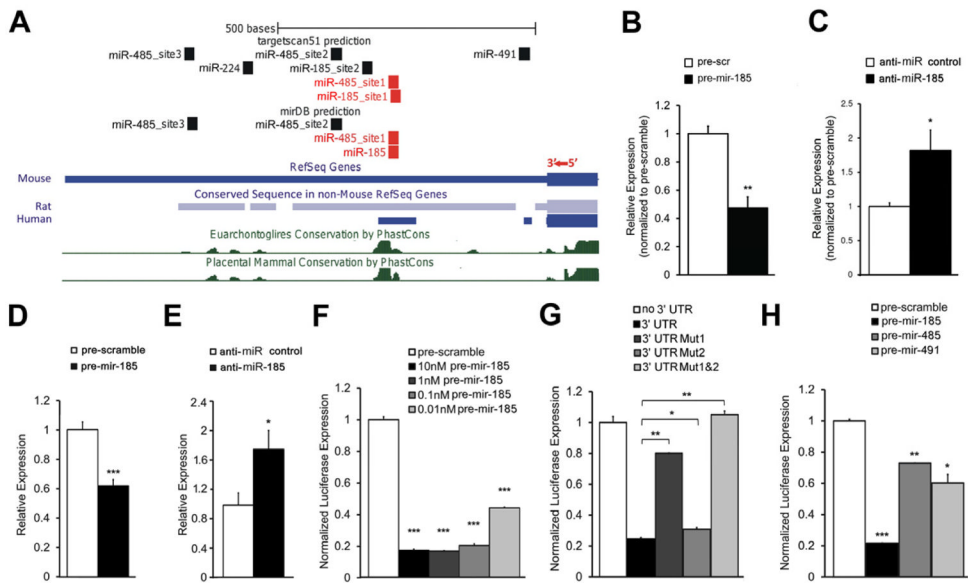


Figure 3. miR-185 directly targets and represses 2310044H10Rik (*Mirta22*)

(A) Structure of the 3'UTR of *2310044H10Rik (Mirta22)* showing miRNA binding sites predicted by TargetScan or mirDB. Blocks in mouse *2310044H10Rik (Mirta22)* 3'UTR that are highly conserved in rat and human orthologues are shown below the mouse 3'UTR. Evolutionary conservation is also assessed by the “30-way multiz alignment and conservation analysis” in the UCSC browser, with conserved blocks indicated by green peaks. miR-185 and miR-485 binding sites located within the conserved blocks are shown in red.

(B, C) qRT-PCR quantification of endogenous *2310044H10Rik (Mirta22)* in DIV7 hippocampal neurons. Expression levels in anti-miR-185-treated and pre-miR-185-treated neurons were normalized to expression levels under respective controls. (B) Increased expression levels of *Mirta22* in neurons transfected with anti-miR-185 at DIV5 ($n = 5$, each treatment). (C) Reduced expression levels of *Mirta22* in DIV9 hippocampal neurons transfected with pre-mir-185 mimic at DIV7 ($n = 3$, each treatment).

(D, E) qRT-PCR quantification of endogenous *2310044H10Rik (Mirta22)* in N18 cells. Expression levels in pre-mir-185-treated and anti-miR-185-treated cells were normalized to expression levels under respective controls. (D) Reduced expression levels of *Mirta22* in cells transfected with pre-mir-185 mimic ($n = 3$, each treatment). (E) Up-regulation of *Mirta22* in cells transfected with an anti-miR-185 LNA oligo ($n = 3$, each treatment).

(F–H) Repression effects of pre-mir-185, pre-mir-485 and pre-mir-491 on *Mirta22* 3'UTR were examined by a dual-luciferase reporter assay (see Methods). Values are *Renilla* luciferase levels relative to firefly luciferase levels and normalized to the relative expression levels under pre-scramble treatment (F, H) or to the relative expression levels from plasmid with no 3'UTR (G) ($n = 3$ for each condition). Pre-mir-185 significantly decreases the *2310044H10Rik (Mirta22)* 3'UTR reporter expression over a concentration range of 10nM to 0.01nM (F). Pre-mir-185 mediated repression on *2310044H10Rik (Mirta22)* 3'UTR reporter expression depends on conserved miRNA binding sites (G). Pre-mir-485 and pre-mir-491 significantly decreases the *2310044H10Rik (Mirta22)* 3'UTR reporter expression (H).

Results are expressed as mean \pm SEM. * $P < 0.05$, ** $P < 0.01$, *** $P < 0.001$ (Student's t -test). See also Figure S3 and Table S3.

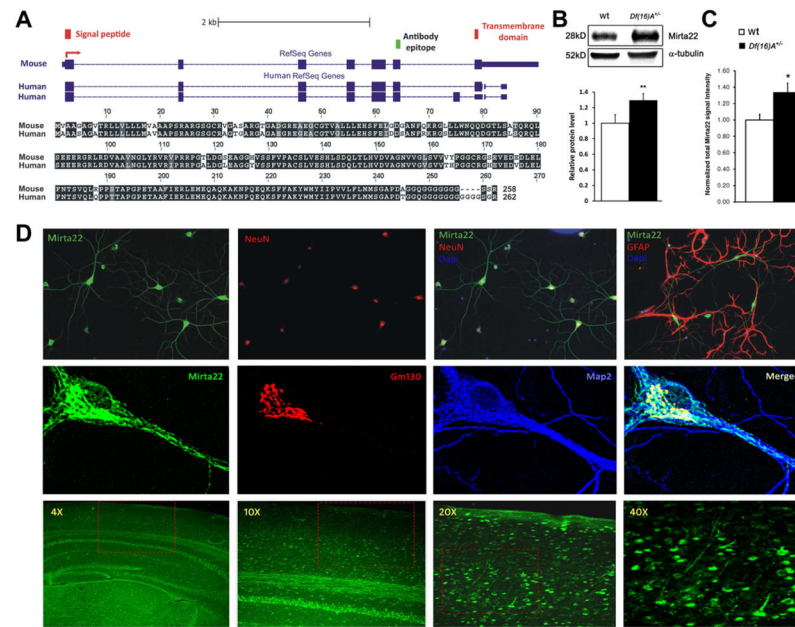


Figure 4. Genomic structure, neuronal expression and subcellular localization of 2310044H10Rik (Mirta22)

(A) *Top*: Structure of mRNA transcripts of *2310044H10Rik* (*Mirta22*) and its human orthologue, *C19orf63*. RefSeq reports a *2310044H10Rik* (*Mirta22*) transcript with 7 exons (blue rectangles), which is predicted to encode a signal peptide and a transmembrane domain (red rectangles). The peptide epitope used to generate a polyclonal antibody is marked by green rectangle. For *C19orf63*, RefSeq reports 2 alternatively spliced transcripts: one that encodes a predicted transmembrane protein and one with an additional exon that encodes a predicted secreted protein. *Bottom*: Protein sequence alignment of predicted transmembrane isoforms encoded by *2310044H10Rik* (*Mirta22*) and its human orthologue. Black blocks indicate completely conserved residues; grey blocks indicate similar residues (defined by Boxshade default similarities); white blocks indicate different residues.

(B) *Upper*: Representative western blot assays of 2310044H10Rik (*Mirta22*) in PFC lysates prepared from *Df(16)A^{+/-}* animals and Wt littermates. Alpha-tubulin is used as loading control. *Lower*: Quantification of 2310044H10Rik (*Mirta22*) protein level in PFC of *Df(16)A^{+/-}* and Wt animals ($n = 9$ each genotype). Expression levels in mutant mice were normalized to Wt littermates. Results are expressed as mean \pm SEM. $**P < 0.01$ (Student's t -test).

(C) Quantification of 2310044H10Rik (*Mirta22*) immunocytochemical signals in *Df(16)A^{+/-}* and Wt cultured neurons ($n = 31$ for *Df(16)A^{+/-}*; $n = 34$ for Wt). Expression levels in mutant neurons were normalized to Wt neurons. Results are expressed as mean \pm SEM. $*P < 0.05$ (Student's t -test).

(D) *Upper panel*: 2310044H10Rik (*Mirta22*) co-localizes with neuron specific marker NeuN, but not with glia specific marker GFAP, in cultured hippocampal neurons at DIV20. *Middle panel*: 2310044H10Rik (*Mirta22*) (green) co-localizes with Golgi specific marker GM130 (red) in the soma. 2310044H10Rik (*Mirta22*) is also found in vesicles and tubular-like clusters in the dendrites, which are highlighted by the dendritic marker MAP2 (blue). *Lower panel*: Distribution of 2310044H10Rik (*Mirta22*) protein in adult mouse brain. Sections were stained with 2310044H10Rik (*Mirta22*) antibody. Images were taken at 4X, 10X, 20X and 40X magnifications as indicated. Red boxes in 4X, 10X, 20X images outline the area shown in 10X, 20X and 40X images, respectively. See also Figure S4.

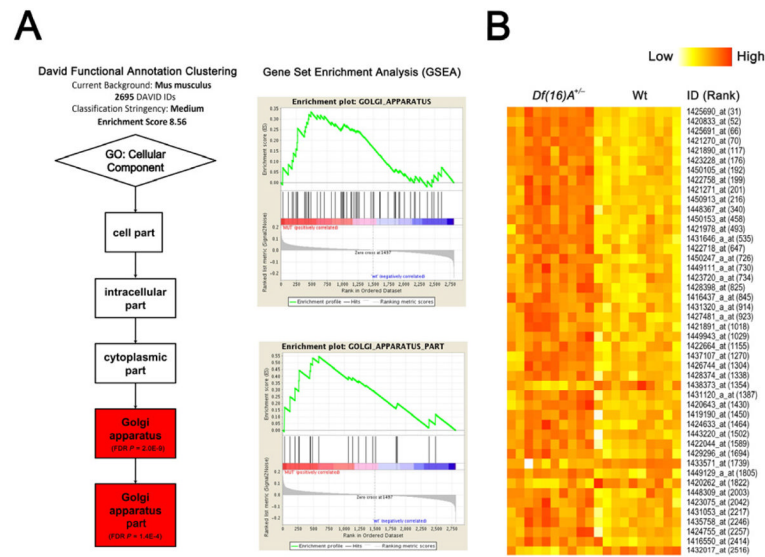


Figure 5. Coordinated mild dysregulation of Golgi-related putative miR-185 targets in *Df(16)A^{+/-}* mice

(A) DAVID functional annotation clustering analysis (left) and Gene Set Enrichment Analysis (GSEA v2.0) (right) of genes predicted as miR-185 targets by TargetScan Mouse v5.2 identified Gene Ontology (GO) terms “Golgi apparatus” and “Golgi apparatus part” as the top enriched gene sets (see Supplemental Methods).

(B) Expression heatmap plot of the potential miR-185 targets that serve Golgi apparatus related functions (GO term) and are differentially expressed ($P < 0.005$) between adult HPC of *Df(16)A^{+/-}* mice and Wt littermates. ID is Affymetrix ID (see Table S4); Rank is the ranking position in the list of all differentially expressed genes according to significance level. Note that the majority (89%, 34 out of 38) of the genes are upregulated. See also Figure S5 and Table S4.

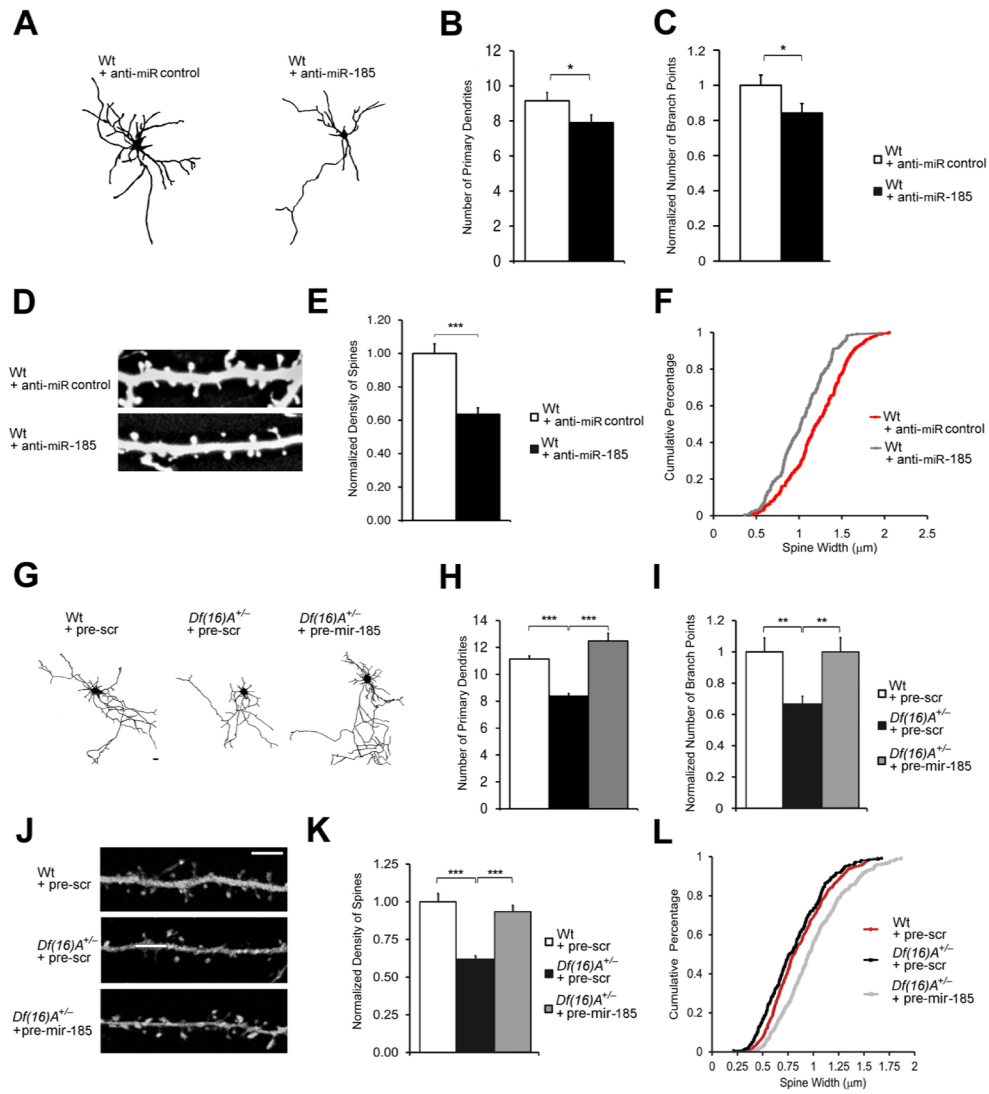


Figure 6. Reduced miR-185 levels contribute to structural alterations of *Df(16)A*^{+/-} neurons

(A) Representative images of Wt neurons at DIV9 transfected with anti-miR control or anti-miR-185 oligos and enhanced GFP.

(B, C) Reduction in the number of primary dendrites (B) and branch points (C) in Wt neurons at DIV9, 2 days after transfection with anti-miR-185 relative to Wt neurons transfected with anti-miR control ($n = 21$ for Wt + anti-miR-185; $n = 20$ for Wt + anti-miR control). In (C), values of Wt + anti-miR-185 were normalized to Wt + anti-miR control.

(D) Representative images of spines on Wt neurons at DIV19, transfected with anti-miR control or anti-miR-185, as well as enhanced GFP.

(E) Reduction in the density of mushroom spines in neurons transfected with anti-miR-185 relative to neurons transfected with anti-miR control ($n = 20$ for Wt + anti-miR-185; $n = 20$ for Wt + anti-miR control). Values of Wt + anti-miR-185 were normalized to Wt + anti-miR control.

(F) Transfection of anti-miR-185 oligos significantly decreased the width of mushroom spines compared to that of the neurons transfected with anti-miR control at DIV19 (15%, $P < 0.001$, Kolmogorov-Smirnov test) ($n = 232$ for Wt + anti-miR-185; $n = 293$ for Wt + anti-miR control).

(G) Representative *Df(16)A^{+/-}* neurons at DIV9 transfected with pre-scramble or pre-mir-185 mimic and enhanced GFP for visualization. Scale Bar, 20 μ m.

(H, I) Reduction in the number of primary dendrites (H) and branch points (I) in *Df(16)A^{+/-}* neurons at DIV9 relative to Wt neurons is reversed by the transfection of pre-mir-185, but not pre-scramble mimic (pre-scr) ($n = 21$ for Wt + pre-scr; $n = 21$ for *Df(16)A^{+/-}* + pre-scr; $n = 21$ for *Df(16)A^{+/-}* + pre-mir-185). In (I), values of *Df(16)A^{+/-}* neurons were normalized to Wt + pre-scr.

(J) Representative images of spines on *Df(16)A^{+/-}* neurons at DIV19, transfected with pre-scramble or pre-mir-185 mimic, as well as enhanced GFP. Scale Bar, 5 μ m.

(K) Reduction in the density of mushroom spines in DIV19 *Df(16)A^{+/-}* neurons relative to Wt control neurons is reversed by the transfection of pre-mir-185, but not pre-scramble mimic, into *Df(16)A^{+/-}* neurons. ($n = 23$ for Wt + pre-scr; $n = 21$ for *Df(16)A^{+/-}* + pre-scr; $n = 23$ for *Df(16)A^{+/-}* + pre-mir-185). Values of *Df(16)A^{+/-}* neurons were normalized to Wt + pre-scr.

(L) Transfection of pre-mir-185 mimic, but not pre-scramble control, significantly increased the width of mushroom spines of *Df(16)A^{+/-}* neurons at DIV19 (18%, $P < 0.001$, Kolmogorov-Smirnov test) ($n = 568$ for Wt + pre-scr; $n = 339$ for *Df(16)A^{+/-}* + pre-scr; $n = 527$ for *Df(16)A^{+/-}* + pre-mir-185).

(B, C, E, H, I, K) Results are expressed as mean \pm SEM. * $P < 0.05$, ** $P < 0.01$ (Student's t -test). See also Figure S6.

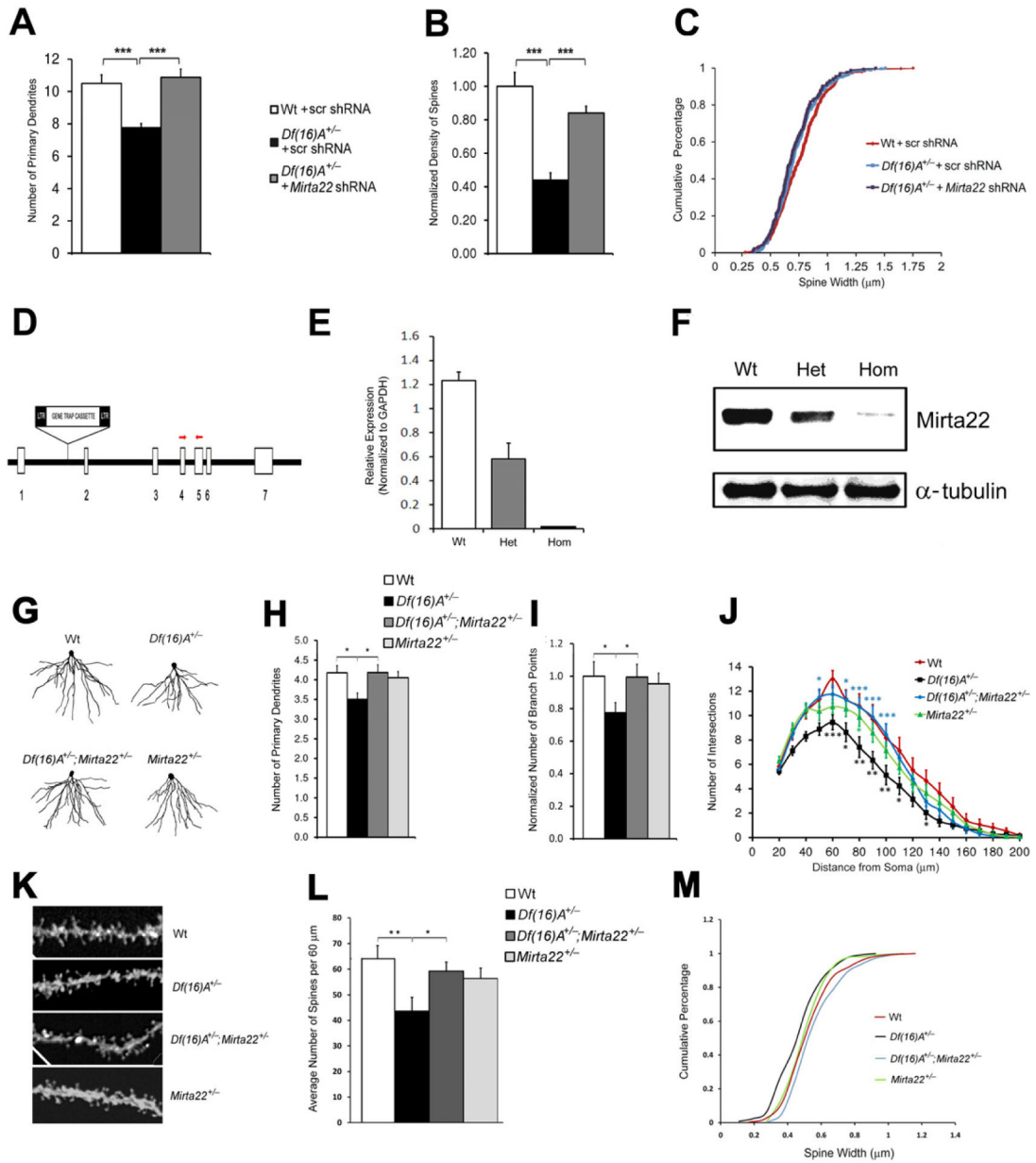


Figure 7. Reduction of *Mirta22* levels reverses structural alterations in the HPC of *Df(16)A^{+/-}* mice *in vitro* and *in vivo*

(A) Reduction in the number of primary dendrites in *Df(16)A^{+/-}* neurons at DIV9 relative to Wt neurons is reversed by the transfection of a construct that expresses *2310044H10Rik* (*Mirta22*) shRNA^{+/-} ($n = 24$ for Wt + scr shRNA; $n = 21$ for *Df(16)A^{+/-}* + scr shRNA; $n = 25$ for *Df(16)A^{+/-}* + *Mirta22* shRNA). Scr shRNA: scramble shRNA.

(B) Reduction in the density of mushroom spines in *Df(16)A^{+/-}* neurons at DIV19 relative to Wt neurons is reversed by the introduction of *Mirta22* shRNA, but not scramble shRNA ($n = 22$ for Wt + scr shRNA; $n = 24$ for *Df(16)A^{+/-}* + scr shRNA; $n = 15$ for *Df(16)A^{+/-}* + *Mirta22* shRNA). Values of *Df(16)A^{+/-}* neurons were normalized to Wt + scr shRNA.

(C) Transfection of *Mirta22* shRNA does not affect the width of mushroom spines of *Df(16)A^{+/-}* neurons at DIV19 ($P > 0.05$, Kolmogorov-Smirnov test). $n = 342$ for Wt + pre-scr; $n = 289$ for *Df(16)A^{+/-}* + pre-scr; $n = 177$ for *Df(16)A^{+/-}* + pre-mir-185.

(D) Schematic (not to scale) of the genomic structure of *Mirta22* depicting the gene-trap insertion in the intron between exons 1 and 2. Red arrowheads indicate approximate genomic location of PCR primers used for qRT-PCR.

(E) *Mirta22* transcript levels in HPC of adult homozygous ($n = 3$) and heterozygous ($n = 3$) *Mirta22* mutant mice as well as their Wt littermates ($n = 3$), as assayed by qRT-PCR.

(F) Representative Western blot assay depicting *Mirta22* protein levels in HPC of adult homozygous ($n = 3$) and heterozygous ($n = 3$) *Mirta22* mutant mice as well as their Wt littermates. Levels of α -tubulin are shown as internal loading controls.

(G) Representative images from diolistic labeling of basal dendrites of CA1 pyramidal neurons from all four tested genotypes. Brains were dissected from 8-wk old littermate mice.

(H, I) Number of primary dendrites (H) and branch points (I) in the basal dendritic tree of CA1 pyramidal neurons from all four tested genotypes ($n = 17$ for Wt; $n = 29$ for *Df(16)A*^{+/-}; $n = 23$ for *Df(16)A*^{+/-};*Mirta22*^{+/-}; $n = 22$ for *Mirta22*^{+/-}). In (I), values of *Df(16)A*^{+/-} and *Df(16)A*^{+/-};*Mirta22*^{+/-} neurons were normalized to Wt neurons.

(J) Sholl analysis of basal dendrite complexity of CA1 pyramidal neurons using 10 μ m concentric circles around the soma. $n = 17$ for Wt; $n = 29$ for *Df(16)A*^{+/-}; $n = 23$ for *Df(16)A*^{+/-};*Mirta22*^{+/-}; $n = 22$ for *Mirta22*^{+/-}. Note that the reduction in branching in *Df(16)A*^{+/-} CA1 neurons is more prominent at the 50–100 μ m range from soma as compared to Wt neurons (black asterisks for Wt versus *Df(16)A*^{+/-} comparison) and it is reversed in the presence of the *Mirta22* mutation (blue asterisks for *Df(16)A*^{+/-} versus *Df(16)A*^{+/-};*Mirta22*^{+/-} comparison).

(K) Representative images of spines at the basal dendrites of CA1 pyramidal neurons from all four tested genotypes. Brains were dissected from 8-wk old littermate mice.

(L) Density of total spines in the basal dendritic tree of CA1 pyramidal neurons from all four tested genotypes. Note that reduction in spine density in *Df(16)A*^{+/-} CA1 neurons is reversed in the compound heterozygous *Df(16)A*^{+/-};*Mirta22*^{+/-} mice. ($n = 14$ for Wt; $n = 6$ for *Df(16)A*^{+/-}; $n = 9$ for *Df(16)A*^{+/-};*Mirta22*^{+/-}; $n = 9$ for *Mirta22*^{+/-}).

(M) Width of mushroom spines (quantified over 60 μ m of dendritic length) in the basal dendritic tree of CA1 pyramidal neurons from all four tested genotypes. Note that reduction in width is reversed in the compound heterozygous mice *Df(16)A*^{+/-};*Mirta22*^{+/-} ($P < 0.001$, Kolmogorov-Smirnov test).

Results are expressed as mean \pm SEM. * $P < 0.05$, ** $P < 0.01$, *** $P < 0.001$ (Student's t -test). See also Figure S7.